Large Disturbance Stability Study of Wind Turbine with DFIG Based on Critical Fault Clearance Time (CFCT)

[1]Ali Asghar Samadi, [1]Samira Asiabi, [2]Morteza Ahmadi and [1]Abdolreza Gharehkhani

[1]Department of Engineering, Minoodasht Branch, Islamic Azad University, Minoodasht, Iran
[2]Department of Engineering, Aliabad Katoul Branch, Islamic Azad University, Aliabad Katoul, Iran

Abstract: As one of the most promising Distributed Generation (DG) sources, wind power technology has been widely developed in recent years. The doubly fed induction generator (DFIG) is currently one of the most common topologies employed for wind turbine generators (WTGs). This generator operates as a synchronous/asynchronous hybrid generators. Therefore, it is necessary to power engineers find understand the characteristics of the DFIG better. This paper is used an analytical method for analysis of large-disturbance stability of DFIG. The proposed analysis is based on the concepts of stable and unstable electrical-mechanical equilibrium points the electrical - mechanical torque versus rotor speed and Critical fault clearance time of DFIG. The results of analysis specified the effective parameters on the large-disturbance stability of DFIG. In other words, this analysis reduces the simulation efforts necessary to assess the large-disturbance stability of DFIG.

Key words: Wind turbine · Doubly fed induction generator (DFIG) · Large-disturbance stability and Critical fault clearance time

INTRODUCTION

The growth of wind energy has continued during the past decade and renewed focus on alternative sources of energy has contributed to its further development worldwide. In some cases, the amount of wind generation has approached that of conventional technologies and the impact of wind on system stability, operation and power quality can no longer be neglected. New recommendations and utility standards require that wind parks aid in voltage support and that turbines remain connected during system disturbances [1]. The doubly fed induction generator variable speed wind turbine introduces itself as a very attractive option for installations with a fast growing market demand. The stator windings are connected directly to network and the back-to-back voltage sourced converters (VSCs) are connected between the supply and the rotor windings. The fundamental feature of the DFIG is that the power processed by the power converter is only a fraction of the total wind turbine power and therefore its size, cost and losses are much smaller compared to a full size power converter [2]. Fig. 1 shows the modern version of the rotor
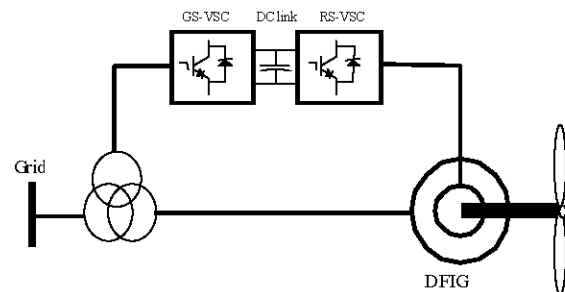

Fig. 1: Variable speed wind turbine with Doubly Fed Induction Generator

controls based on two IGBT Voltage-source converters (VSCs). The rotor speed does not have to be constant and can vary with the wind velocity even though the stator is generating power at 50 or 60 Hz. Since this generator operate as the wind turbine connected to network, hence it is necessary to are studied performance of DFIG on the normal and fault operation conditions. An important phenomenon related to the DFIG operation that deserves special attention is its dynamic behavior during faults. due to the abrupt reduction in the electrical torque on during short circuits DFIG may accelerate to high speeds.
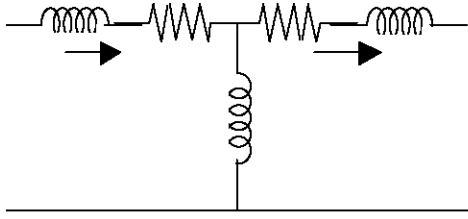
Corresponding Author: Ali Asghar Samadi, Department of Engineering, Minoodasht Branch,
Islamic Azad University, Minoodasht, Iran. E-mail: a.a.samadi@birjand.ac.ir.

Fig. 2: Electrical equivalent circuit of DFIG

Fig. 3: Approximate equivalent circuit of DFIG

Therefore on during fault the reactive power consumed by the DFIG increases considerably, however, within the available current capacity the Line Side Converter can be controlled to participate in reactive power generation on during fault periods [3]. Thus, the large-disturbance stability phenomena of DFIG can be verified by analyzing the dynamic response of the rotor speed or the terminal voltage during faults p eriod. The large-disturbance stability of DFIG has been intensively investigated by using dynamic simulations [4] or even experimental tests [5]. On the other hand, little effort has been carried out to analyze such phenomenon by using analytical methods. Therefore, the main purpose of this paper is the presentation of effective parameter on the large-disturbance stability of DFIG. The impact of effective parameters is studied base on steady states circuit of DFIG and balance point of electrical- mechanical torque versus rotor speed. This research reduces the studies of computer dynamic simulations of DFIG under normal and fault operation conditions.

Steady State Equvalent Circuit of Dfig: Fig. 2 shows the well-known Steady Sate Equivalent Circuit of DFIG. The conventional motor direction of stator current I_s and rotor current I_r is adopted. On the stator side, R_s and $j\omega_s L_{s1}$ are the resistance and leakage reactance. On the rotor side, R_r and $j\omega_s L_{r1}$ are the resistance and leakage reactance of the rotor winding. The mutual reactance is $j\omega_s M$. When the rotor rotates at angular velocity of ω_m electrical radian/s, the rotor resistance R_r is modified as R_r / s where $s = (1- \omega_m / \omega_s$ is the slip. The rotor-side Voltage Source Converter of Fig. 1 injects balanced three-phase voltages (v_{Ra}, v_{Rb}, v_{Rc}) at slip frequency $\omega_r = s\omega_s$, voltage magnitude V_R and voltage angle δ. Because Fig. 2 is based on the stator-side frequency ω_s, the VSC voltage phasor $V_R = V_R \angle \delta$ representing (v_{Ra}, v_{Rb}, v_{Rc}) has also to be divided by the slip s resulting in the equivalent rotor voltage $V_R = V_R / s \angle \delta$ [6].
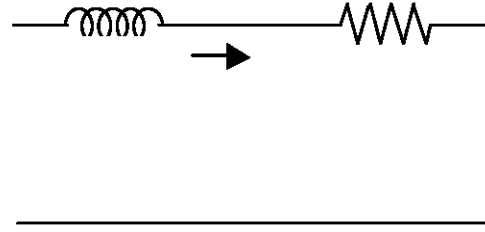
Steady Sate Torque Equation of Dfig: In order to understanding the performance characteristics and a facile solution finding for the torque equation of DFIG, Fig. 2 can be simplified to Fig. 3 which considers the large mutual reactance $j\omega_s M$ to be virtually an open circuit. In the approximation in Fig.3, the impedance $Z_s = R + jX$ where:

$$Z_s = R_s + \frac{R_r}{s} + j(\omega_s L_{s1} + \omega_s L_{r1}) = R + jX \qquad (1)$$

When the stator excitation is $V_S = V_S \angle 0$ and the rotor excitation is $V_R = V_R / s \angle \delta$, the rotor current is:

$$I_r = \frac{V_s \angle 0 - V_r \angle \delta}{Z_s} \qquad (2)$$

Of the rotor-side voltage $1/s(I_r R_r + V_R)$, one deducts two

Voltage Terms: $I_r R_r$, the voltage drop across the rotor resistance and $V_R = V_R / s \angle \delta$, the voltage output of the VSC of the rotor-side voltage. The voltage, which is left after the deduction, is associated with electromechanical energy conversion:

$$E_m = (I_r R_r + V_R)\left(\frac{1}{s} - 1\right) \qquad (3)$$

By applying $s = (1 - \dot{u}m/\dot{u}S)$ in Eq (3):

$$E_m = (I_r R_r + V_R)\frac{\omega_m}{s\omega_s} \qquad (4)$$

Multiplying both sides Eq (3) by I_r^*, where * is the complex conjugate operator, the electrical power is converted to mechanical power through the equation:

$$T_e \omega_m = \text{Re}(E_m I_r^*) = \text{Re}\left(I_r^* (I_r R_r + V_R)\frac{\omega_m}{s\omega_s}\right) \qquad (5)$$

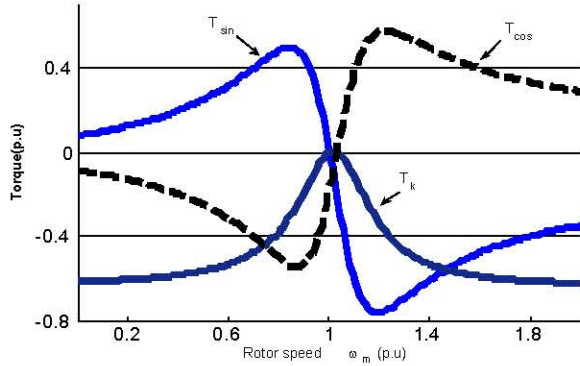Where T_e is the electromechanical torque. Substituting I_r and dividing both sides by ω_m.

Fig. 4: Electrical torque versus of rotor speed of DFIG

$$T_e = \frac{\mathrm{Re}\left(I_r^*\left(I_r R_r + V_R\right)\right)}{s\omega_s}$$

$$= \frac{\mathrm{Re}\left(\dfrac{V_s\angle 0 - V_r\angle -\delta}{Z_s^*}\left(\dfrac{V_s\angle 0 - V_r\angle \delta}{Z_s}R_r + V_R\right)\right)}{s\omega_s} \quad (6)$$

After simplified the electromechanical torque equation (6), for easily in writing, the electromechanical torque equation is divided into 3 terms [6].

$$T_e = T_k + T_{\sin} + T_{\cos} \quad (7)$$

That

$$T_k = \frac{V_s^2}{\left|Z_s\right|^2 \omega_s}\frac{R_r}{s} - \left(\frac{V_R}{s}\right)^2 \frac{R_s}{\left|Z_s\right|^2 \omega_s} \quad (8)$$

$$T_{\cos} = -\left(\frac{V_R}{s}\right)\frac{V_s\left(\dfrac{R_r}{s} - R_s\right)}{\left|Z_s\right|^2 \omega_s}\cos\delta \quad (9)$$

$$T_{\sin} = -\left(\frac{V_R}{s}\right)\frac{V_s\left(X_{rl} + X_{sl}\right)}{\left|Z_s\right|^2 \omega_s}\sin\delta \quad (10)$$

Fig. 4 Is showed alternations of the three terms torque equations (8)-(9) versus rotor speed.

Critical Rotor Speed of Dfig: During the occurrence of short circuits in the network, DFIG tend to accelerate due to the abrupt reduction in the electrical torque. Thus, the large-disturbance stability of a DFIG can be determined by analyzing the response in the time of the rotor speed after the short-circuit application. The unstable performance of DFIG will depend on the fault
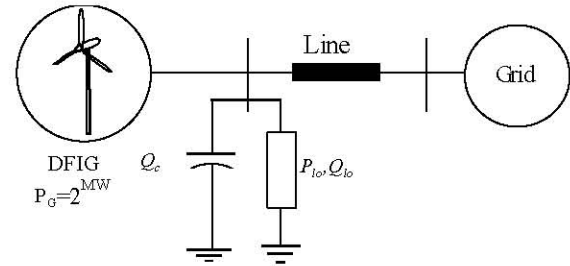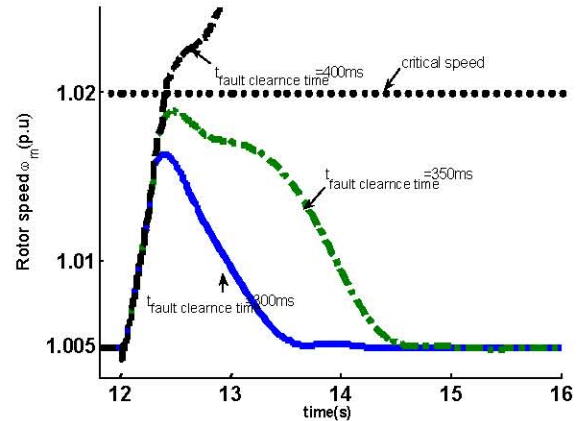

Fig. 5: Case study system

Fig. 6: Rotor speed of DFIG on the different fault Clearance Time

clearance time. More specifically, it will depend on whether the fault will be eliminated before the generator rotor speed reaches the maximum critical speed. The concept of critical speed of induction generators was first proposed in [7] and further analyzed in [8]. As an illustrative example, the test system presented in Fig. 5 will be used to briefly revise the concept of critical speed through dynamic simulation. This test system is composed by a 2MW, DFIG connected by a line to a 20kV, 50Hz substation. In addition, at the DFIG bus, there is a Q_c Mvar capacitor bank and a P_{lo}, Q_{lo} local load. The system parameters are specified in the Appendix. In order to explain the concept of critical speed, a three-phase short circuit is applied to the DFIG bus at 12 s. The rotor speed responses for different fault clearance time are presented in Fig. 6.

This figure reveals that when the short circuit is eliminated in or faster than 350 ms, the DFIG does not lose its stability. Otherwise, when the fault clearance time is longer than 400ms, the DFIG becomes unstable. Thus, the critical fault clearance time for this case is 350 ms. Another interpretation of these results is as follows. When the fault is eliminated before the rotor speed reaches 1.02 p.u., the DFIG does not lose its stability. Otherwise, when the fault is eliminated after the rotor speed reaches 1.02 p.u.,
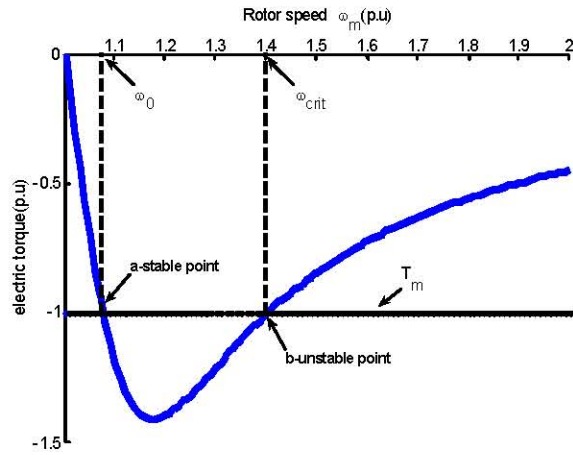
Fig. 7: Electrical torque versus of rotor speed of DFIG on the generator mode

Fig. 8: Stable performance of DFIG base on electrical torque curve

the generator becomes unstable. Therefore, the critical rotor speed (or simply the critical speed) for this case is 1.02 p.u. [9].

The Critical Fault Clearance Time Calculation of Dfig: In this section, the method of The Critical fault Clearance Time Calculation of DFIG is explained. In order to facilitate the explanations, first, the method is applied and developed to a simple system composed by an DFIG directly connected to an infinite bus. Later, in this section, the method is generalized to be applied to more complex systems.

The concept of critical rotor speed can be further explained by using the electrical torque versus rotor speed curve of a DFIG in specific condition. In order to obtain a mathematical relationship between electrical torque and rotor speed, the steady-state equivalent circuit of DFIG that shown in Fig. 2 can be used [7]. When the DFIG operates as a generator, the mechanical torque T_m is negative. Therefore, the electrical–mechanical equilibrium equation of DFIG can be written as:

$$\frac{d\omega_m}{dt} = \frac{1}{2H}(T_e - T_m) \tag{11}$$

Where H is the inertia constant. By using (7), the electrical torque versus rotor speed curve can be plotted as shown in Fig. 7.

From Fig. 7, two equilibrium points, where the electrical torque is equal to the mechanical torque, can be found. It is easy to show that the equilibrium point represented **a** by is the stable one and the equilibrium point represented by **b** is the unstable one.
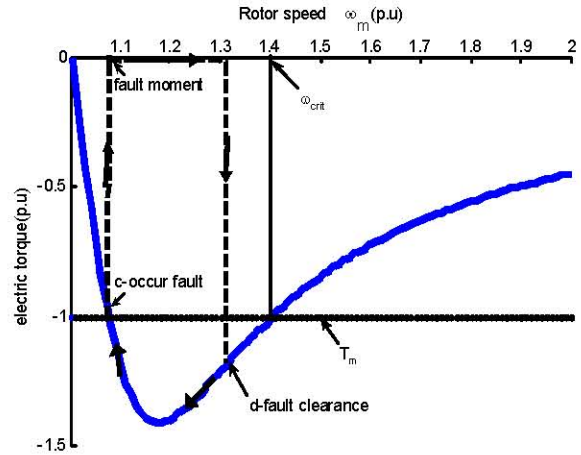
The rotor speed at **a** point is the steady-state speed ω_0 in which the DFIG normally operates. In addition, the rotor speed at point is the critical speed ω_{crit}. This can be better explained by using Figs. 8 and 9, where the system trajectory is shown considering two different fault clearance times.

In Fig. 8, before the fault occurrence, the DFIG is operating at point **c**, where the rotor speed is ω_0. At this instant, a fault is applied and the electrical torque abruptly decreases to zero. As a result, the rotor speed starts to increase governed by (11). At instant t_d, the fault is eliminated and the DFIG operating point changes to **d**. At this instant, the rotor speed starts to decrease since the net torque $T_e - T_m$ is negative and eventually the DFIG will return to operate at point **c**.

On the other hand, in Fig. 9, before the fault occurrence, the DFIG is operating at point **e**. At this instant, a fault is applied and the electrical torque abruptly decreases to zero. As a result, the rotor speed starts to increase governed by (11). At instant t_f, the fault is eliminated and the DFIG operating point changes to **f**. At this instant, the rotor speed continues to increase since the net torque $T_e - T_m$ is positive and eventually the DFIG will become unstable [8]. Thus, it can be verified that when the fault is eliminated before the rotor speed reaches the critical speed, the DFIG response is stable. Otherwise, when the fault is eliminated after the rotor speed reaches the critical speed, the DFIG response is unstable. Thus, from the previous explanation, it is possible to calculation of the critical fault clearance time by solving (7) and (11) as follows. The stable and unstable equilibrium points can be determined by making $T_e = T_m$ in (7). Thus, one has
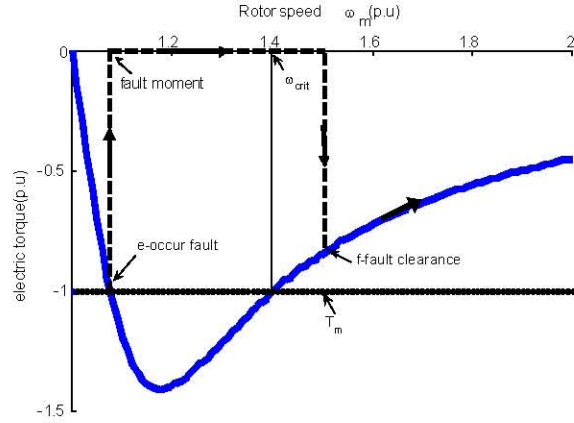
Fig. 9: Stable performance of DFIG base on electrical torque curve

$$as^2 + bs + c = 0, \quad a = T_m \omega_s (R_s^2 + X^2),$$
$$b = 2T_m \omega_s R_s R_r - R_s V_s^2 - V_r V_s (X \sin \delta - R_s \cos \delta) \quad (12)$$
$$c = T_m \omega_s R_r^2 + R s V_r^2 + V_r V R_r \cos \delta$$

This is a second-order equation of s. By solving this equation, one can calculate the steady-state speed ω_0 and the critical speed ω_{crit} by

$$\omega_0 = 1 - \frac{b + \sqrt{\Delta}}{2a} \quad (13)$$

$$\omega_{crit} = 1 - \frac{b - \sqrt{\Delta}}{2a} \quad (14)$$

Where is $\Delta = b^2 - 4ac$. Substituting (13) and (14) in the solution of (11), one can calculate the critical fault clearance time. At instant fault, $T_e = 0$ therefore Eq (11) by

$$\frac{dt}{d\omega_m} = \frac{2H}{(-T_m)} \quad (15)$$

The Critical fault Clearance Time is calculated By integrate the two sides of Eq. (15) in interval the steady state speed ω_0 through critical speed ω_{crit}.

$$t_{crit} = \frac{2H}{(-T_m)} \int_{\omega_0}^{\omega_{crit}} d\omega_m = \frac{2H}{(-T_m)}(\omega_{crit} - \omega_0) = \frac{2H}{(-T_m)}$$
$$\frac{1}{T_m \omega_s (R_s^2 + X^2)} \sqrt{\Delta} \quad \Delta = b^2 - 4ac \quad (16)$$

Generalized the Critical Fault Clearance Time Calculation for Bulk Power System: In order for the study to be more useful, it must be applicable to more
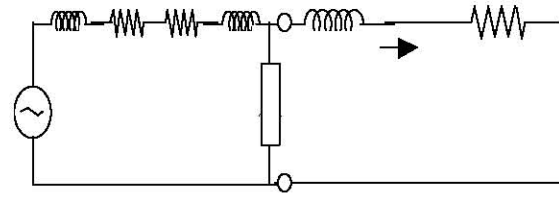

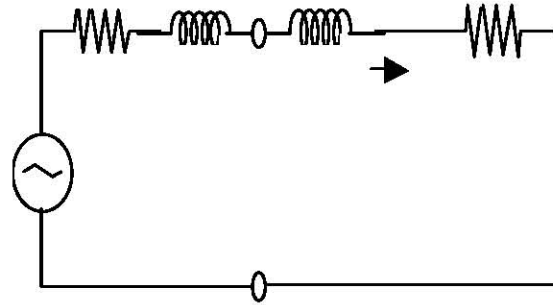Fig. 10: Electrical equivalent circuit of the case study system

Fig. 11: Simplified equivalent circuit of the case study system

generic systems than that represented in Fig. 3. Indeed, the study can be applied to any complex system by using the Thevenin Theorem. The test system presented in Fig. 5 will be used as an example here. This system can be represented by the equivalent electrical circuit shown in Fig. 10. In this figure, R_{Grid}, jX_{Grid} are the grid resistance and reactance, respectively, R_{lime}, X_{lime} are the line resistance and reactance, respectively and $Z_L = 1/(P_{lo} + j(Q_{lo} - Q_c))$ is the equivalent impedance that represents the local active power load, the local reactive power load and the local capacitor bank and. * is the complex conjugate operator. The electrical circuit shown in Fig. 10 can be easily reduced to the equivalent circuit presented in Fig. 11, where the new Thevenin voltage V_{TH} and the Thevenin impedance $Z_{TH} = R_{TH} + jX_{TH}$ can be calculated by

$$V_{TH} = \frac{Z_L}{Z_{Grid} + Z_{line} + Z_L} V_{Grid} \quad (17)$$

$$Z_{TH} = R_{TH} + jX_{TH} = \frac{(Z_{Grid} + Z_{line})Z_L}{Z_{Grid} + Z_{line} + Z_L} \quad (18)$$

That Z_{grid}, Z_{lime} are the equivalent impedances of grid and line respectively. The circuit shown in Fig. 11 can be easily reduced to the circuit shown in Fig. 3 by substituting Z_s by $Z_{TH} + Z_s$ and V_s by V_{TH}.

As a result, expressions (2), (7) and (11)-(16) are still valid to the complete system. Thus, the large-disturbance stability of the DFIG can be inferred by knowing only the substation voltage and the machine and system parameters and by using (16). It is to worth pointing out that any linear network can be reduced to the equivalent circuit shown in Fig. 11 Consequently, the analytical method can be easily applied to complex distribution systems composed by several loads, transformers and feeders.

Impact of Effective Parameter on the Critical Fault Clearance Time: In this section, several machine and network parameters are varied and, for each variation, the critical fault clearance time is calculated by repeated by using (11). The parameters varied were: stator and rotor resistance, rotor and stator reactance, line length, local reactive power compensation level, local load level, substation and rotor voltage level and rotor voltage angle δ. This sensitivity study permits widely validating the analytical method and determining the main factors that affect the large-disturbance stability of DFIG. In addition, the range of parameter variation is not necessarily intended to cover only typical parameter values.

Impact of Dfig Parameters: In this subsection, the main parameters of the DFIG are varied. Fig. 12 shows the influence of the rotor and stator resistance on the critical fault clearance time. This figure reveals that the value of the stator resistance does not have much influence on the induction generator stability performance. On the other hand, the increase of the rotor resistance has a very positive impact on the induction generator stability performance. Therefore, on the fault ride through condition of DFIG, the protection system can make short circuit the rotor terminal by crowbar and variation rotor resistant improves system stability. Thus, it may be recommendable to increase the rotor resistance in order to improve the generator stability performance that the rotor losses increase. Another notice, by considering (13)-(14), that when the rotor resistance increases, the steady-state speed also increases which is harmful to the stability; however, the critical speed also increases, which is beneficial to the stability. Since the critical speed increases more than the steady-state speed, the net effect is beneficial to the stability.
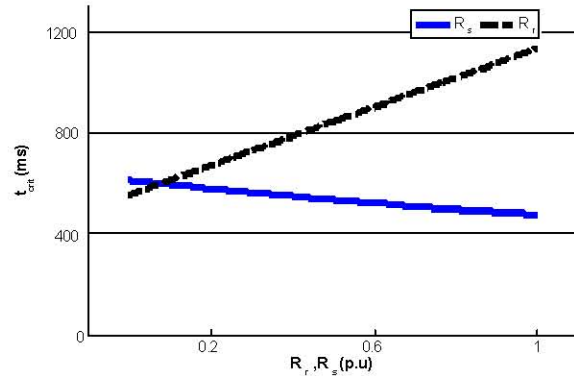

Fig. 12: The impact of the rotor and stator resistance on the critical fault clearance time
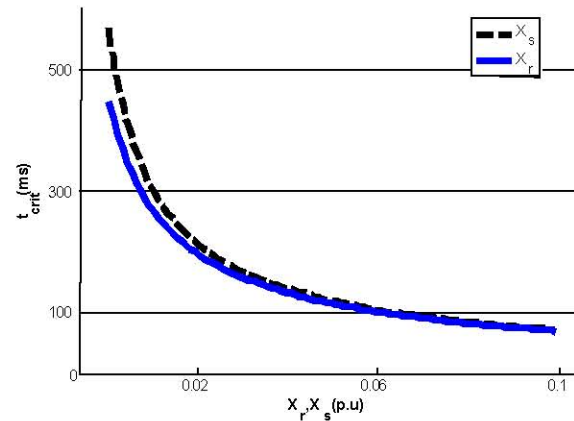

Fig. 13: The impact of the rotor and stator reactance on the critical fault clearance time

Fig. 13 shows the influence of the stator and rotor reactances on the critical fault clearance time. This figure, obtained directly from the application of (16). In addition, this figure reveals that, the value of the stator and rotor reactances has a great impact on the induction generator stability. One can see that the smaller the stator and rotor reactances are, the higher the critical fault clearance time. These facts can be explained by analyzing the influence of these parameters on the steady-state speed and on the critical speed by using (13) and (14). Thus, during the project of DFIG, the minimization of the stator and rotor reactances are fundamental to improve the DFIG stability.

The influence of the variation of the stator and rotor voltage level the critical fault clearance time is analyzed in Fig. 14 the variations limit to 1.25p.u. From this figure, one can see that the higher the stator and rotor voltage level are, the higher the critical fault clearance time is. The explanations for the previously commented impacts can be better understood by (13) and (14). From figure the impact of the variation of the stator voltage is higher than
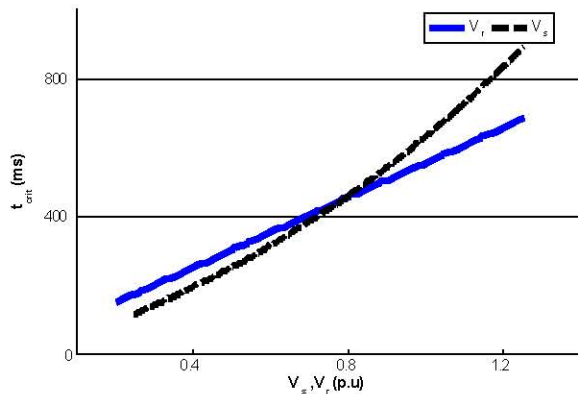
Fig. 14: The impact of the rotor and stator voltage on the critical fault clearance time
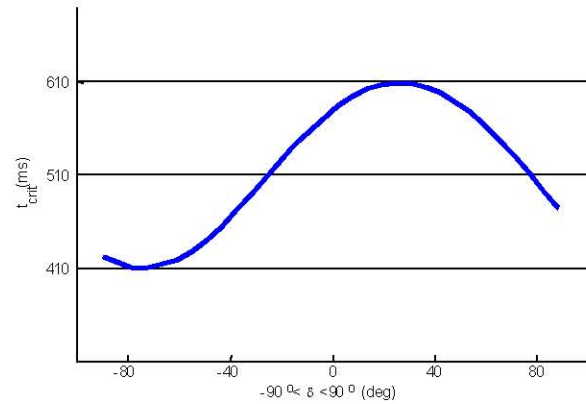

Fig. 16: The impact of the phase angle of the rotor voltage on the critical fault clearance time
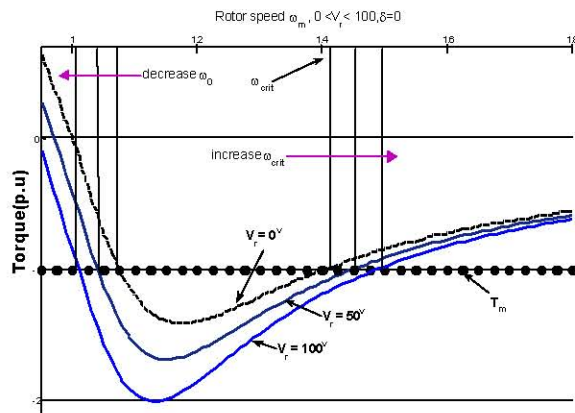

Fig. 15: The impact of the rotor voltage on the torque characteristic
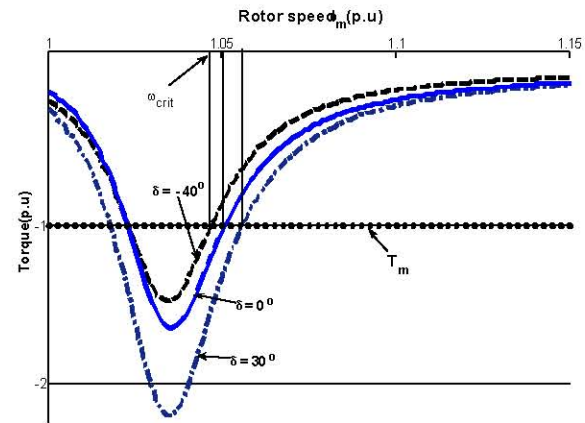

Fig. 17: The impact of the phase angle of the rotor voltage on the torque characteristic

Fig. 18: The impact of line length on the critical fault clearance time

variation of the rotor voltage at interval of 0.8-1.25 p.u but, since the voltage stator is fixed by network hence it is easy to changes the rotor voltage level. Fig. 15 shows impact of the variation of the rotor voltage on the torque characteristic of DFIG. This figure is obtained for the variation of the rotor voltage 0-100 Volt and the phase angle δ=0. The important notice from this figure reveals, it is that in addition the critical speed increase, which is beneficial to the stability, the steady-state speed decreases. Hence by the rotor voltage control of DFIG, stability of system are increased.

Fig. 16 Shows the influence of the phase angle δ of the rotor voltage for $-90 < \delta < 90$ on the critical fault clearance time. The curve of torque versus rotor speed for $\delta = 30°, 0°, -40°$ is shown in Fig. 17. This figure verified results of Fig. 16 from Fig. 16 reveals that the critical fault clearance time increase for positive of the phase angle δ. Hence stability of DFIG improves by applying the control of the rotor voltage phase angle.
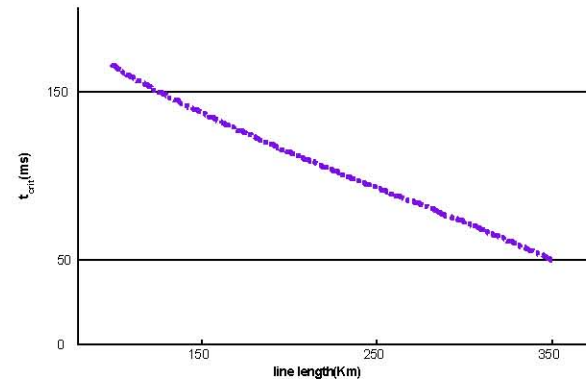
Impact of Network Parameters: In this subsection, the impacts of network parameters are varied. Fig. 18 shows the impact of the line length on the stability. This figure reveals that the longer the line is, the smaller the critical fault clearance time is. This observation is in accord with
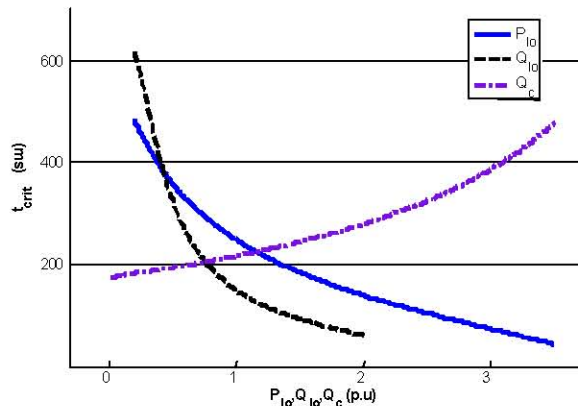
Fig. 19: The impact of P_{lo}, Q_{lo}, Q_c on the critical fault clearance time

the conclusion that a weak power system, which presents a high line impedance and, consequently, a low short-circuit level at the DFIG connection point, has a small stability margin. In the long line for solution this problem, suitable compensators use.

The impact of the local load level and the local reactive power compensation level on the generator stability performance are shown in Fig. 19, where the local load and local reactive power compensation are given in per unit at the generator power base. This figure shows that when the local load level increases, the critical fault clearance time decreases and can see that the higher the local reactive power compensation is, the higher the critical fault clearance time is.

CONCLUSION

This paper is used an analytical method for analysis of large-disturbance stability of DFIG. The proposed analysis is based on the concepts of stable and unstable electrical-mechanical equilibrium points the electrical - mechanical torque versus rotor speed and Critical fault clearance time of DFIG. The rotor speed and the Critical fault clearance time are selected as criteria. results of study are determined the effective parameters on the large-disturbance stability of DFIG. Results of paper can be used on the design and protection projects.

The control of the phase angle and level of the rotor voltage of DFIG is distinguished from another squirrel cage induction generator. By applying this property, DFIG can be operates as synchronous generator.

REFERENCES

1. Chad, Abbey and G´eza Jo´os, 2008. A systematic approach to design and operation of a doubly fed induction generator, Electric Power Systems Res., 78 399-408

2. Pena, R., J.C. Clare and G.M. Asher, 1996. Doubly fed induction generator using back-to-back PWM converters and its application to variable-speed wind energy generation, J. Proc. Electr. Power Appl., 43(3).

3. Ekanayake, J.B., L. Holdsworth, X. Wu and N. Jenkins, 2003. Dynamic modeling of doubly fed induction wind turbines, J. IEEE Trans. Power Syst., 8(2).

4. Najafi, H.R., F. Robinson, A.A. Samadi and F. Dastyar, 2008. The impact of electric wind farm operation with Doubly Fed Induction Generator (DFIG) on electric power grid, ICEE Japan.

5. Mora, E.S., T.I.A. Olivares, D.R. Veja and D.O. Salinas, 2002. The effect of induction generators on the transient stability of a laboratory electric power system, Elect. Power Syst. Res., 61: 211-219.

6. Doubly-fed Induction Generator (DFIG) as a Hybrid of Asynchronous and Synchronous Machines Lianwei Jiao a, B.Ooi b, G. Jo´os b, F. Zhoub, Electric Power Systems Res., 76(2005) 33-37.

7. Akhmatov, V., H. Knudsen, M. Bruntt, A.H. Nielsen, J.K. Pedersen and N.K. Poulsen, 2000. A dynamic stability limit of grid-connected induction generators, in Proc, IASTED Int. Conf. Power and Energy, Marbella, Spain, pp: 235-244.

8. Grilo, A., A. Mota, L. Mota and W. Freitas, 2007. An Analytical Method for Analysis of Large-Disturbance Stability of Induction Generators, Ieee Transactions on Power Systems, 22(4).

9. Akhmatov, V., 2003. Analysis of dynamic behaviour of electric power systems with large amount of wind power, Ph.D. dissertation, Tech. Univ. Denmark, Lyngby.